

# Q-LIC: Quantizing Learned Image Compression with Channel Splitting

Heming Sun, Lu Yu, and Jiro Katto

**Abstract**—Learned image compression (LIC) has reached a comparable coding gain with traditional hand-crafted methods such as VVC intra. However, the large network complexity prohibits the usage of LIC on resource-limited embedded systems. Network quantization is an efficient way to reduce the network burden. This paper presents a quantized LIC (QLIC) by channel splitting. First, we explore that the influence of quantization error on the reconstruction error is different for various channels. Second, we split the channels whose quantization has larger influence to the reconstruction error. After the splitting, the dynamic range of channels is reduced so that the quantization error can be reduced. Finally, we prune several channels to keep the number of overall channels as origin. By using the proposal, in the case of 8-bit quantization for weight and activation of both main and hyper path, we can reduce the BD-rate by 0.61%-4.74% compared with the previous QLIC. Besides, we can reach better coding gain compared with the state-of-the-art network quantization method when quantizing MS-SSIM models. Moreover, our proposal can be combined with other network quantization methods to further improve the coding gain. The moderate coding loss caused by the quantization validates the feasibility of the hardware implementation for QLIC in the future.

**Index Terms**—Learned image compression, quantization, fixed-point, channel splitting

## I. INTRODUCTION

IMAGE compression is important to relieve the burden of the image transmission and storage. In the past decades, several standards have been developed such as JPEG [1], JPEG2000 [2], WebP [3] and HEVC intra (BPG) [4]. For these standardized methods, the coding components are fixed which are composed of intra prediction, linear transform, quantization and entropy coding. To improve the coding gain, new features such as more intra modes and larger transform kernels have been developed. However, the coding components are optimized separately thus the joint optimization might lead to a higher compression ratio. In addition, the transform kernels such as discrete cosine transform (DCT) are performed linearly, thus adopting the non-linear feature is potential for improving the compression ability.

In the recent years, learned image compression (LIC) has illustrated a superior compression ability. One classical LIC framework is hyper-prior model [5] which is composed of main path and hyper path. Main path is served as a non-linear transform, while hyper path is used for the entropy coding. Based on the hyper-prior framework, there have been quite a

few of works [6]–[11] improving the coding gain by enhancing the transform ability in the main path and attempting more sophisticated entropy model in the hyper path. As a result, the recent LIC work [8] can reach a comparable coding gain with the latest traditional standard VVC intra [12].

Along with a considerable coding gain improvement, the network complexity of LIC also increases hugely as reported in [13]. First, to store and transfer a huge amount of parameters and activations, the memory consumption is high. Second, the arithmetic operation of weights and activations is computationally intensive when using 32-bit floating point. To alleviate the above two problems, network pruning and quantization are two mainstream approaches. By using the pruning methods in [14]–[17], some weights and activations are cut so that the memory consumption can be saved. However, the computational cost in the worst case still remains the same as origin which requires the 32-bit floating-point multiplier and adder. By using the quantization methods, the bit-depth of weights and activations is reduced to save the memory consumption. Moreover, the computational burden can also be relieved. As a result, quantized model can be mapped on some specific hardwares [18]–[22] for the acceleration.

Network quantization can be grouped to two categories according to the quantization targets. First category is to quantize the weight. Han *et al.* [23] clustered weights and then applied a non-uniform quantization. An incremental network quantization scheme was proposed in [24] and the key concept was to quantize the partial weights and then compensate the quantization loss by fine tuning the remaining weights recursively, until all the weights have been quantized. Vector quantization was utilized to compress the weights in [25]. Lipschitz constraint-based width-level and multi-level network quantization were proposed for high-bit and low-bit quantization respectively in [26].

Second category is focused on the activation quantization. Park *et al.* [27] presented value-aware quantization so that lower quantization precision (QP) is applied to smaller values. The author also exploited the concept of weighted entropy and analyzed the impact of different weight/activation value on the final accuracy in [28]. Mishra *et al.* [29] proposed a low precision network providing more filters than the origin which can surpass the accuracy of the baseline full-precision network. There are also several works emphasizing on optimizing the activation range. Jung *et al.* [30] determined the efficient activation interval by learning the center and distance parameter. Variants of ReLU with different bounding value and piece-wise function was proposed in [31]. Batch normalization [32] was utilized to purposely generate a Gaussian-like distri-

Heming Sun is with Waseda University, Japan and JST, Japan. (heming-sun@aoni.waseda.jp)

Lu Yu is with Zhejiang University, China. (yul@zju.edu.cn)

Jiro Katto is Waseda University, Japan. (katto@waseda.jp)



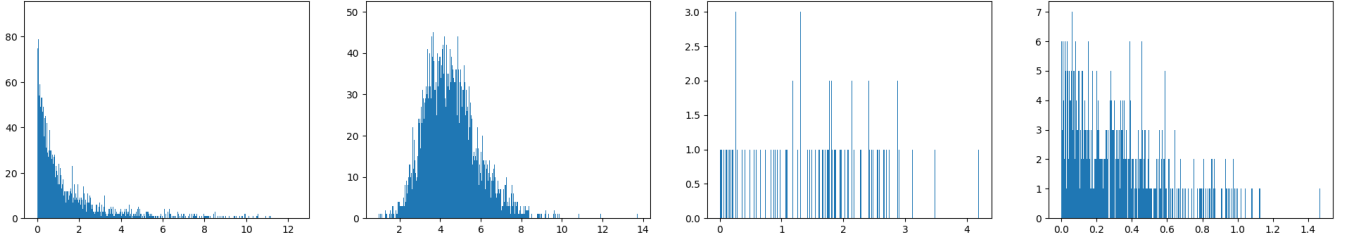


Fig. 2. Activation distribution for four channels of  $g_a^{(0)}$ . There is no unified distribution for various channels, and dynamic range also varies for different channels.

error, each value has its own  $t$ . To reduce the storage burden, all the values can share one  $t$ . Considering the structural feature of convolution neural network, appropriate grouping scheme for  $t$  can be performed in the channel-wise or layer-wise.

### B. Quantized LIC

In this work, we build the baseline network based on the *hyperprior-5* model in [41] as shown in Fig. 1. There are four layers in the main analysis transform  $g_a$  and synthesis transform  $g_s$  respectively as described in the following equation

$$\mathbf{y} = g_a(\mathbf{x}) = g_a^{(3)} \circ g_a^{(2)} \circ g_a^{(1)} \circ g_a^{(0)}(\mathbf{x}) \quad (2)$$

$$\hat{\mathbf{x}} = g_s(\hat{\mathbf{y}}) = g_s^{(3)} \circ g_s^{(2)} \circ g_s^{(1)} \circ g_s^{(0)}(\hat{\mathbf{y}}) \quad (3)$$

where  $\hat{\mathbf{y}} = \lfloor \mathbf{y} \rfloor$ . The hyper path can be formulated as below

$$z = h_a(\hat{\mathbf{y}}) \quad (4)$$

$$\boldsymbol{\mu}_y, \boldsymbol{\sigma}_y = h_s(\hat{z}) \quad (5)$$

where  $\hat{z} = \lfloor z \rfloor$ . For the activation function, ReLU and Leaky-ReLU rather than the generalized divisive normalization (GDN) [42] is used to ease the hardware implementation in the future. The slope of Leaky-ReLU is set as 0.125 which can be operated as right shifting.

The target of this paper is to quantize the weights and activations of all the layers. About the weight quantization, previous work [39] has illustrated that linearly quantizing to 8-bit will not lead to large coding loss. About the activation quantization, quantizing the hyper path will not cause coding loss as reported in [37], [39]. Therefore, the remaining issue is to quantize the activation in the main path, including both bottleneck layer and non-bottleneck layers.

For the outputs of bottleneck layer  $g_a^{(3)}$ , without any bit-budget limitation, it is just rounded thus the quantization precision is one. In the case of limited bit-budget, in order not to clip the dynamic range, the quantization precision can be decided by the following equation.

$$s = \begin{cases} 1, & \text{if } 2^{\lceil \log 2^t \rceil} < 2^{b-1} \\ \frac{2^{\lceil \log 2^t \rceil}}{2^{b-1}}, & \text{if } 2^{\lceil \log 2^t \rceil} \geq 2^{b-1} \end{cases} \quad (6)$$

For the outputs of non-bottleneck layers, one distribution instance for  $g_a^{(0)}$  is shown in Fig. 2. We can see that there is no obvious distribution shape, thus we use LQ rather than NLQ. Besides, the dynamic range of various channels are different, so channel-wise rather than layer-wise quantization is adopted.

## III. RELATIONSHIP BETWEEN QUANTIZATION ERROR AND R-D COST

### A. Reconstruction Error for Linear System

According to [43], for the linear sub-band coding system, when quantizing the outputs of analysis transform, we have the following relationship

$$\sigma_r^2 = \sum_{k=0}^{K-1} B_k \sigma_{q_k}^2 \quad (7)$$

where  $\sigma_{q_k}^2$  is the variance of the quantization error and  $\sigma_r^2$  is the variance of the reconstruction error,  $K$  is the number of channels. By substituting the approximate relationship [44],

$$\sigma_{q_k}^2 \simeq \epsilon_k^2 2^{-2b_k} \sigma_{y_k}^2 \quad (8)$$

where  $y_k$  is the outputs of analysis transform,  $\epsilon_k$  is related with the distribution of  $y_k$  and  $\sigma_{y_k}$  is the variance of  $y_k$ ,  $b_k$  is the quantization bit for each channel.

### B. Reconstruction Error for Quantized LIC

LIC has two differences from linear sub-band coding system. First difference is that LIC is a non-linear system when using non-linear activation functions. Second difference is that in [43], only the outputs of the bottleneck layer are quantized, while outputs of both bottleneck layer and non-bottleneck layer are quantized in our quantized LIC.

For the  $g$ -th non-bottleneck layer, the relationship between the variance of the quantization error and the variance of the reconstruction error can be written as below.

$$\sigma_{r^{(g)}}^2 = \sum_{k=0}^{K-1} B_k^{(g)} \sigma_{q_k^{(g)}}^2 \quad (9)$$

To evaluate  $B_k$ , in addition to the bottleneck layer, we also quantize the  $k$ -th channel of the  $g$ -th layer. In this case, the reconstruction error can be written as

$$\sigma_r^2 = B_k^{(g)} \sigma_{q_k^{(g)}}^2 + \sigma_{r^{(g_a^{(3)})}}^2 \quad (10)$$

where  $\sigma_{r^{(g_a^{(3)})}}^2$  is the reconstruction error caused by quantizing the bottleneck layer. We quantize the  $k$ -th channel with five different quantization bits, and obtain  $B_k$  by the linear regression. Results are shown in Fig. 3. We can see that  $B_k$  for various channels are different. Large  $B_k$  means that the quantization error will have more influence to the reconstruction error.

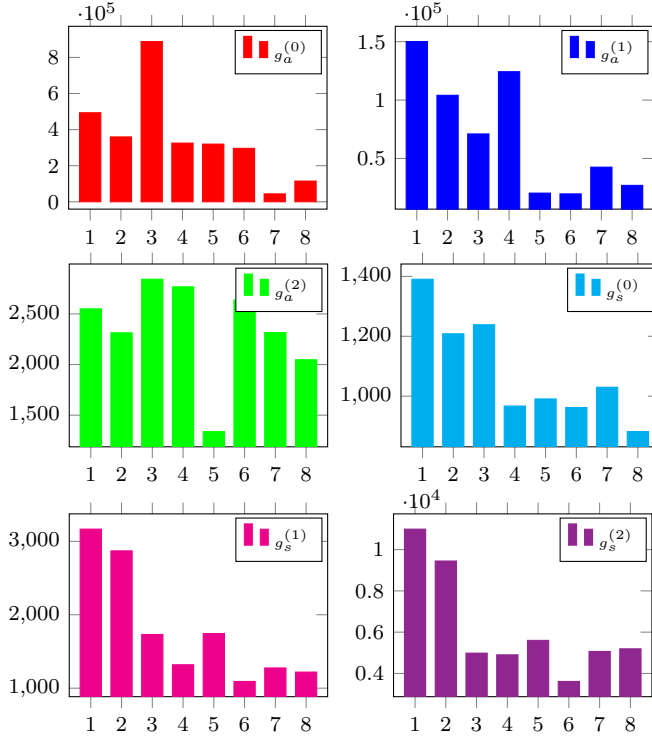


Fig. 3.  $B_k$  for eight channels with the largest energy of different non-bottleneck layers.

Now that when quantizing each individual layer, the quantization influence to the reconstruction error of each channel can be evaluated by  $B_k$ , then we explore the quantization influence of each layer to the reconstruction error when quantizing multiple layers. We first quantize the  $g$ -th non-bottleneck layer as well as the bottleneck layer to obtain  $\sigma_{r(g)}^2$  as below.

$$\sigma_{r(g)}^2 = \sigma_r^2 - \sigma_{r(g^{(3)})}^2 \quad (11)$$

After that, we quantize all the layers to obtain reconstruction error  $\sigma_r^2$ . The relationship between  $\sum_{g \in G} \sigma_{r(g)}^2$  and  $\sigma_r^2$  is shown in Fig. 4. From the results, we can clarify that the reconstruction error caused by quantizing each layer can be simply accumulated as below

$$\sigma_r^2 = \sum_{g \in G} \sigma_{r(g)}^2 + \sigma_{r(g^{(3)})}^2 \quad (12)$$

where  $G$  is all the non-bottleneck layers including  $g_a^{(0,1,2)}$  and  $g_s^{(0,1,2)}$ . Therefore, to reduce the overall reconstruction error, we should reduce the quantization error for each layer.

### C. Rate-Distortion for Quantized LIC

The relationship between the quantization error and reconstruction error has been given in the above. We analyze Rate-distortion (R-D) cost in this section. R-D cost is calculated by

$$J = R + \lambda D \quad (13)$$

where  $R$  is the rate and  $D$  is the distortion. In the case of distortion being MSE, given that the reconstruction error is a

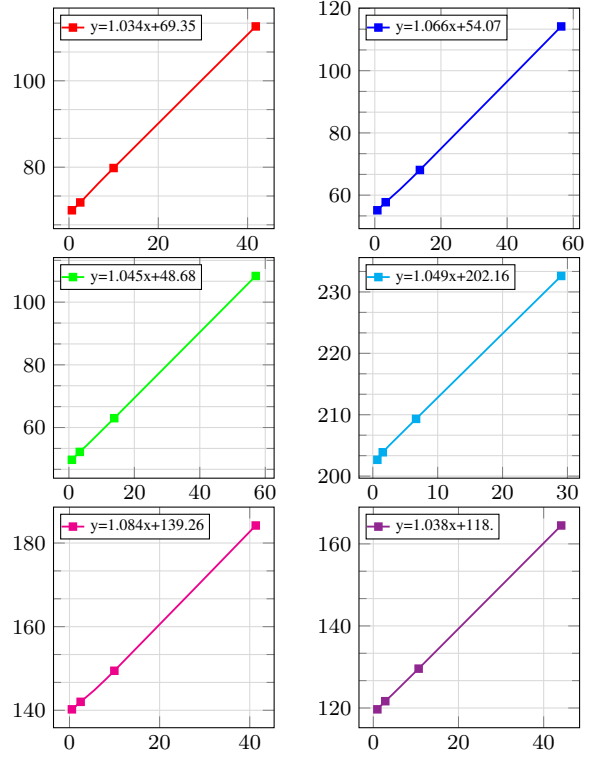


Fig. 4. The relationship between  $\sum_{g \in G} \sigma_{r(g)}^2$  and  $\sigma_r^2$ .  $G$  includes all the non-bottleneck layers.

zero-mean uniform distribution,  $\sigma_r^2$  can be directly used as the distortion. Therefore, R-D cost can be rewritten as

$$\begin{aligned} J &= R + \lambda \sigma_r^2 \\ &= R + \lambda \left( \sum_{g \in G} \sigma_{r(g)}^2 + \sigma_{r(g^{(3)})}^2 \right) \\ &= J_0 + \lambda \sum_{g \in G} \sigma_{r(g)}^2 \\ &= J_0 + \lambda \sum_{g \in G} \sum_{k=0}^{K-1} B_k^{(g)} \sigma_{q_k}^2 \end{aligned} \quad (14)$$

where the former part  $J_0$  is the R-D cost in the case of only quantizing the bottleneck layer and the latter part represents the R-D cost increase when quantizing the non-bottleneck layers.

In the case of distortion being  $1 - \text{MS-SSIM}$ , the relationship between  $\sigma_r^2$  and MS-SSIM in the case of quantizing different layers are shown in Fig. 5. We can see that the relationship can be approximated as below.

$$\text{MS-SSIM} \simeq -a\sigma_r^2 + 1 \quad (15)$$

where  $a$  is a positive value. Therefore, R-D cost can be rewritten as

$$\begin{aligned} J &\simeq R + \lambda a \sigma_r^2 \\ &= J_0 + \lambda a \sum_{g \in G} \sum_{k=0}^{K-1} B_k^{(g)} \sigma_{q_k}^2 \end{aligned} \quad (16)$$

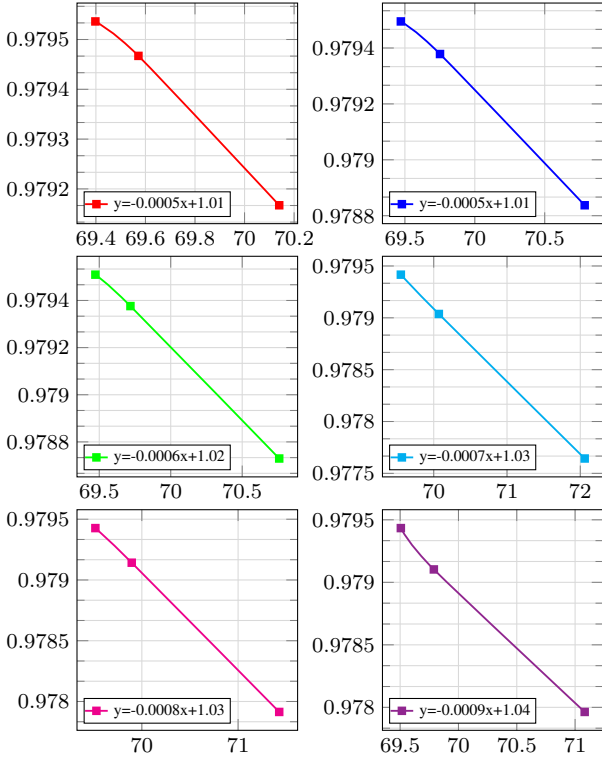


Fig. 5. The relationship between  $\sigma_r^2$  and MS-SSIM for different layers.

From Eq. 14 and Eq. 16, we can see that when quantizing multiple layers in addition to the bottleneck layer, R-D cost increase is proportional to the quantization error.

Regarding the rate, it will not be changed if we quantize the synthesis transform. However, rate will be different from the non-quantized baseline if we quantize the analysis transform. According to our experimental results, when using 8-bit to quantize the analysis transform, there is no big change for the rate. In addition, rate can be reduced by fine tuning the hyper path. Therefore, we assume that the quantization does not influence the rate in the above derivation.

#### IV. PROPOSED CHANNEL SPLITTING

As described in the previous section, reducing the quantization error for each layer can contribute to a better coding gain. By splitting the channel, the dynamic range can be shrunk so that the quantization error can be reduced.

In this section, we formulate the channel splitting problem at first, and then propose the channel splitting methods for non-bottleneck and bottleneck layer respectively. In order not to increase the network burden, some channels are pruned. Finally, we present the overall framework to illustrate the procedures of channel splitting and pruning.

##### A. Channel Splitting Formulation

For the  $i$ -th layer, the activation output is  $\mathbf{O}_i \in \mathbb{R}^{w_i \times h_i \times c_i}$  where  $w_i$  and  $h_i$  are the width and height, and  $c_i$  is the number

of the output channels. For the  $n$ -th channel  $\mathbf{O}_i^{(n)} \in \mathbb{R}^{w_i \times h_i}$ , it is calculated by

$$\mathbf{O}_i^{(n)} = \sum_{m=0}^{C_{i-1}} \mathbf{O}_{i-1}^{(m)} * \mathbf{W}_i^{(m,n)} + \mathbf{b}_i^{(n)} \quad (17)$$

where  $m$  and  $n$  are the index of input and output channel,  $\mathbf{O}_{i-1}$  is the output of the previous layer,  $\mathbf{W}_i^{(m,n)}$  and  $\mathbf{b}_i^{(n)}$  are weight and bias.

Given that a specific channel  $\mathbf{O}_i^{(n)}$  is split to  $\mathcal{K}$  channels  $\mathbf{O}_i'^{(n_k)}$ , each split channel can be calculated by the following equation.

$$\mathbf{O}_i'^{(n_k)} = \sum_{m=0}^{C_{i-1}} \mathbf{O}_{i-1}^{(m)} * \mathbf{W}_i'^{(m,n_k)} + \mathbf{b}_i'^{(n_k)} \quad (18)$$

To ensure that the network function does not change after the splitting, we should have the following relationship.

$$\sum_{k=0}^{\mathcal{K}-1} \mathbf{O}_i'^{(n_k)} = \mathbf{O}_i^{(n)} \quad (19)$$

To satisfy Eq. 19, the weight and bias for the split channels are set as below

$$\mathbf{W}_i'^{(:,n_k)} = \frac{\mathbf{W}_i^{(:,n)}}{\mathcal{K}} \quad (20)$$

$$\mathbf{b}_i'^{(n_k)} = \frac{\mathbf{b}_i^{(n)}}{\mathcal{K}} + \delta_k \quad (21)$$

where  $:$  is a wild card for all the input channels, and  $\delta_k$  is a small offset to generate various quantized value for split channels. As long as  $\sum_{k=0}^{\mathcal{K}-1} \delta_k = 0$ , we can satisfy Eq. 19 based on Eq. 20 and Eq. 21.

The split output channels of the  $i$ -th layer are also the input channels of the  $i+1$ -th layer. Therefore, not only  $\mathbf{W}_i'^{(:,n_k)}$  but also  $\mathbf{W}_{i+1}'^{(m_k,:)}$  should be defined. Here  $m_k$  for the  $i+1$ -th layer is equal to  $n_k$  for the  $i$ -th layer. The definition for  $\mathbf{W}_{i+1}'^{(m_k,:)}$  is shown in Eq. 22 where  $:$  is the wild card for all the output channels.

$$\mathbf{W}_{i+1}'^{(m_k,:)} = \mathbf{W}_{i+1}^{(m,:)} \quad (22)$$

Based on Eq. 19 and Eq. 22, we can have the following relationship which means that the channel splitting for the  $i$ -th layer will not influence the results of the  $i+1$ -th layer.

$$\sum_{k=0}^{\mathcal{K}-1} \mathbf{O}_i'^{(m_k)} * \mathbf{W}_{i+1}'^{(m_k,:)} = \mathbf{O}_i^{(m)} * \mathbf{W}_{i+1}^{(m,:)} \quad (23)$$

##### B. Channel Splitting for Non-bottleneck Layers

Before splitting, each activation output  $x$  is quantized as  $\lfloor \frac{x}{s} \rfloor \cdot s$  where  $s$  is the original quantization precision.

$$x \rightarrow Q(x; s) = \lfloor \frac{x}{s} \rfloor \cdot s \quad (24)$$

After splitting one channel to  $\mathcal{K}$  channels, each activation output  $x_k$  is quantized as  $\lfloor \frac{x_k}{s'} \rfloor \cdot s'$  where  $s'$  is the quantization precision for the split channels.

$$x_k \rightarrow Q(x_k; s') = \lfloor \frac{x_k}{s'} \rfloor \cdot s' \quad (25)$$

According to Eq. 19-21,  $x$  and  $x_k$  have the following relationship so that the dynamic range of split channels can

be reduced by  $\mathcal{K}$  times compared with the original non-split channel.

$$x_k = \frac{x}{\mathcal{K}} + \delta_k \quad (26)$$

Therefore, in the case of same bit budget, the quantization precision for the split channels can be increased by  $\mathcal{K}$  times.

$$s' = \frac{s}{\mathcal{K}} \quad (27)$$

When we set  $\delta_k = (\frac{1}{2\mathcal{K}} + \frac{k}{\mathcal{K}} - \frac{1}{2}) \cdot \frac{s}{\mathcal{K}}$ , the summation of  $Q(x_k; s')$  for the split  $\mathcal{K}$  channels can be derived as

$$\begin{aligned} & \sum_{k=0}^{\mathcal{K}-1} \lfloor \frac{x_k}{s'} \rfloor \cdot s' \\ = & \sum_{k=0}^{\mathcal{K}-1} \lfloor \frac{x + \delta_k \cdot \mathcal{K}}{s} \rfloor \cdot s' \\ = & \sum_{k=0}^{\mathcal{K}-1} \lfloor \frac{x}{s} + \frac{1}{2\mathcal{K}} + \frac{k}{\mathcal{K}} \rfloor \cdot s' \\ = & \lfloor \mathcal{K} \cdot (\frac{x}{s} + \frac{1}{2\mathcal{K}}) \rfloor \cdot s' = \lfloor \frac{x}{s'} \rfloor \cdot s' \end{aligned} \quad (28)$$

where the second last equation in Eq. 28 follows [45]. Here we can see that by splitting to  $\mathcal{K}$  channels, the effect is exactly same as increasing the quantization precision by  $\mathcal{K}$  times for the original channel, which proves that the channel splitting can reduce the quantization error.

Though channel splitting can reduce the quantization error, the number of channels is increased so that the network complexity becomes higher. Therefore, we only split the channels whose quantization error will influence more to the coding gain. The detail framework is shown in Section IV-D.

### C. Channel Splitting for Bottleneck Layer

Before splitting, each activation output  $y$  is rounded to  $\lfloor y \rfloor$ . After splitting one channel to  $\mathcal{K}$  channels, each activation output  $y_k$  is rounded to  $\lfloor y_k \rfloor$ . When we set  $\delta_k$  as  $\frac{1}{2\mathcal{K}} + \frac{k}{\mathcal{K}} - \frac{1}{2}$ ,  $\lfloor y \rfloor$  and  $\lfloor y_k \rfloor$  have the following relationship.

$$\begin{aligned} & \sum_{k=0}^{\mathcal{K}-1} \lfloor y_k \rfloor \\ = & \sum_{k=0}^{\mathcal{K}-1} \lfloor \frac{y}{\mathcal{K}} + \delta_k \rfloor \\ = & \sum_{k=0}^{\mathcal{K}-1} \lfloor \frac{y}{\mathcal{K}} + \frac{1}{2\mathcal{K}} + \frac{k}{\mathcal{K}} \rfloor \\ = & \lfloor \mathcal{K} \cdot (\frac{y}{\mathcal{K}} + \frac{1}{2\mathcal{K}}) \rfloor = \lfloor y \rfloor \end{aligned} \quad (29)$$

We can see that the summation of  $\lfloor y_k \rfloor$  is equal to  $\lfloor y \rfloor$ , which means that the splitting will not influence the coding gain.

Similar as traditional DCT, there are some low-frequency channels with large magnitude in the bottleneck layer. As a result, if the dynamic range is larger than  $2^{b-1}$ , the quantization precision will be larger than one according to Eq. 6. To ensure that the dynamic range is smaller than  $2^{b-1}$ , each specific channel can be split to  $\mathcal{K}$  channels.

$$\mathcal{K} = \frac{\max(2^{\lceil \log 2^{t_c} \rceil}, 2^{b-1})}{2^{b-1}} \quad (30)$$

Overall, for the bottleneck layer, the number of incremental channels after the splitting can be calculated as below

$$\sum_{c=0}^{C_b-1} \frac{\max(2^{\lceil \log 2^{t_c} \rceil}, 2^{b-1}) - 2^{b-1}}{2^{b-1}} \quad (31)$$

where  $C_b$  is the number of channels in the bottleneck layer and  $t_c$  is the dynamic range for each original channel.

It is noted that after splitting  $g_a^{(3)}$ , according to Eq. 22, we need to modify the weights of  $h_a^{(0)}$  to ensure that the outputs of  $h_a^{(0)}$  will not be changed. As a result, the hyper decoder outputs the original  $\mu, \sigma$  which is not aligned with  $\lfloor y_k \rfloor$ . To address this issue, in the encoding side, we calculate  $\sum_{k=0}^{\mathcal{K}-1} \lfloor y_k \rfloor$  and then use  $\mu, \sigma$  to code the summation result. In the decoding side, we first do the entropy decoding to generate the summation  $\sum_{k=0}^{\mathcal{K}-1} \lfloor y_k \rfloor$ , and then split to  $\lfloor y_k \rfloor$  as the input of synthesis transform  $g_s$ .

### D. Overall Framework

For a specific layer, supposed that there are  $S$  incremental channels after the channel splitting. In order not to increase the overall network complexity, we need to prune the same number of channels. To reduce the coding loss caused by the pruning, we prune the channels with the smallest energy. With larger  $S$ , more channels will be split so that the quantization error can be reduced. On the other hand, pruning more channels will cause more coding loss. As a result, we need to find an appropriate  $S$  to balance the coding gain of splitting and pruning.

The overall framework is shown in *Algorithm 1*. Based on a pre-trained model, for the non-bottleneck layer, the optimal  $S$  can be decided by comparing the R-D cost. R-D cost in the case of quantizing each individual layer is shown in Fig. 6. The horizontal axis is the number of channels which are split to two channels, and the vertical axis is the corresponding R-D cost. We can see that R-D cost for the last five cases can be decreased at first, which means that the coding gain due to the channel splitting is larger than the coding loss caused by the channel pruning. However, when we further split more channels, R-D cost increases since the coding loss from channel pruning will become larger than the coding gain by the channel splitting. For the first case, R-D cost without any channel splitting is the lowest. Therefore, the number of channels for the splitting is set as 0.

For the bottleneck layer, the number of incremental channels after the splitting is shown in Eq. 31. To remain the overall number of channels, the same number of channels with the smallest energy will be pruned.

Noted that the output of  $g_a^{(3)}$  is not only the input of  $g_s^{(0)}$ , but also the input of  $h_a^{(0)}$ . Therefore, after splitting the channels of  $g_a^{(3)}$ , we need to define the weights of  $g_s^{(0)}$  as well as  $h_a^{(0)}$  as shown in Eq. 22.

## V. EXPERIMENTAL RESULTS

### A. Training and Network Details

Same as previous works, we train the network with the rate-distortion cost function  $J = R + \lambda \cdot D$ . The distortion term in the loss is  $\text{MSE}(x, \hat{x})$  when optimizing PSNR,

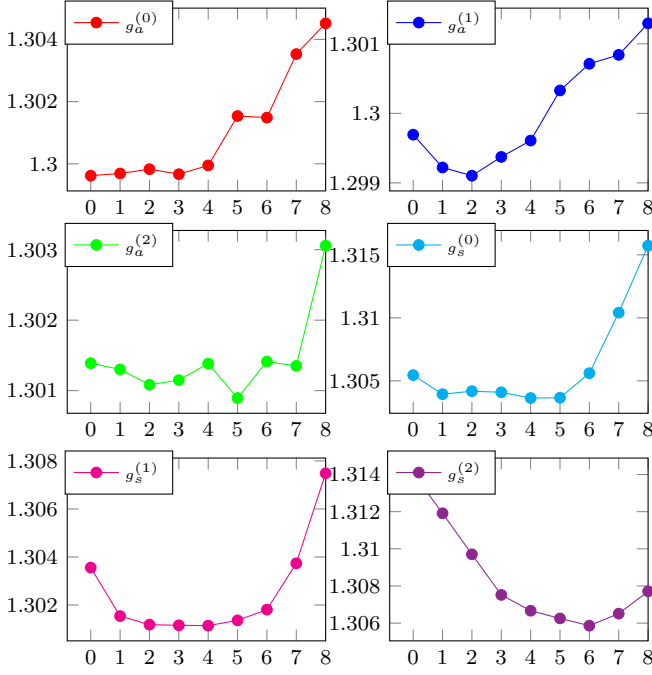


Fig. 6. R-D cost in the case of quantizing each individual layer. Horizontal axis is the number of channels for splitting and pruning, and vertical axis is the corresponding R-D cost. The optimal number of channels for the splitting is 0,2,5,4,4,6 for each layer respectively.

#### Algorithm 1 Overall Framework

- 1: Non-bottleneck layer list  $\mathcal{L}_{nb} = [g_a^{(0,1,2)}, g_s^{(0,1,2)}]$
- 2: Bottleneck layer list  $\mathcal{L}_b = [g_a^{(3)}]$
- 3: Pre-trained model:  $M$
- 4: **Decide split channels  $\hat{S}_{nb}$  for non-bottleneck layers**
- 5: **for**  $l$  in  $\mathcal{L}_{nb}$  **do**
- 6:   Calculate channel-wise energy  $\mathcal{E}_k$  and  $B_k$
- 7:   **for**  $S$  in range(16) **do**
- 8:     Split  $\text{argmax} B[:S]$  channels
- 9:     Prune  $\text{argmin} \mathcal{E}[:S]$  channels
- 10:     Calculate R-D cost  $J(S)$
- 11:   **end for**
- 12:    $\hat{S}_{nb} = \text{argmin}_S J(S)$
- 13: **end for**
- 14: **Decide split channels  $\hat{S}_b$  for the bottleneck layer**
- 15:  $\hat{S}_b = \sum_{c=0}^{C-1} \frac{\max(2^{\lceil \log 2^c \rceil}, 2^{b-1}) - 2^{b-1}}{2^{b-1}}$
- 16: **Split and prune the pre-trained model  $M$**

and it is 1-MS-SSIM( $x, \hat{x}$ ) when optimizing the MS-SSIM. Since different  $\lambda$  can achieve various trade-off between distortion and rate, we train several models to obtain a R-D curve. When optimizing MSE,  $\lambda$  is selected from  $\{0.001625, 0.00325, 0.0075, 0.015, 0.03, 0.05\}$ . When optimizing MS-SSIM,  $\lambda$  is picked up from  $\{3, 5, 10, 40, 80, 128\}$ . To get the baseline pre-trained model in *Algorithm 1*, we train about  $1 \times 10^6$  iterations, the learning rate is set as  $1 \times 10^{-4}$  at first and decayed to  $1 \times 10^{-5}$  for the final 80K iterations.

To decide  $\hat{S}_{nb}$  and  $\hat{S}_b$  in *Algorithm 1*, we randomly picked up nine images from ImageNet. For the test set, we use 24 lossless Kodak images [46] which are commonly used in the previous works. Noted that there is no overlap between the training set and the test set.

TABLE I  
BD-RATE (%) COMPARED WITH THE NON-QUANTIZED FLOAT-POINT BASELINE. SMALLER BD-RATE MEANS THAT THE CODING LOSS DUE TO THE QUANTIZATION IS SMALLER.

	weight	activation	MSE model	MS-SSIM model
Ours	8bit	8bit	4.98	4.34
[39]	8bit	8bit	5.59	9.08
[40]	8bit	10bit	26.5	N/A
[40]	8bit	16bit	17.9	N/A

#### B. Coding Gain Analysis

We compare the coding gain with two recent QLIC works [39], [40]. For [39], the author remained the activation in the main path unquantized. When quantizing the activation in the main path to 8-bit, the results are shown in Fig. 8. Compared with [39], the BD-rate [47] compared with the floating-point anchor can be reduced by 0.61% (5.59-4.98) and 4.74% (9.08-4.34) for MSE model and MS-SSIM model respectively. We can achieve more coding gain for MS-SSIM model since there are more channels for the splitting and pruning by following *Algorithm 1*.

[40] also gave the BD-rate compared with the floating-point anchor for the MSE-optimized model. In the case of 8-bit weight quantization and 10-bit activation quantization, BD-rate is 26.5%. In the case of 8-bit weight quantization and 16-bit activation quantization, BD-rate is 17.9%. Compared with [40], our coding loss caused by the quantization is much smaller.

[37] also illustrate that there will be a coding loss after the quantization. However, the bit-width of weight and activation is not given in the paper. For the fairness, we did not compare with [37] here.

In addition to the comparison with [39], [40], we also give an ablation study when using our proposal for the activation quantization in the main path. The results are shown in Fig. 7. We explore the case of 7-bit and 8-bit quantizations. For the 8-bit quantization, we evaluate four largest bitrate models. For the 7-bit quantization, we evaluate four medium bitrate models. Two datasets are used for the evaluation. We can see that the coding gain improvement for the 7-bit quantization is larger than that for the 8-bit quantization. Besides, we can enhance more coding gain for the MS-SSIM models than the MSE models, and this phenomenon is similar as Fig. 8.

#### C. Effect of Quantization Method

By using the proposal, we can reduce the coding loss of activation quantization without network fine tuning. In fact, our method can be combined with any fine tuning methods to further reduce the coding loss. We evaluate two largest bitrate models of MSE models and MS-SSIM models respectively. Two different bit-width are used in the experiment. From the results in Table II, we can see that [36] can reach better coding gain than our proposal when quantizing MSE models. However, when combining our method with [36], we can achieve lower R-D cost than [36]. For the MS-SSIM models, we can achieve much better coding gain than [36]. In addition, the combination of proposal and [36] can also lead to a further improvement.

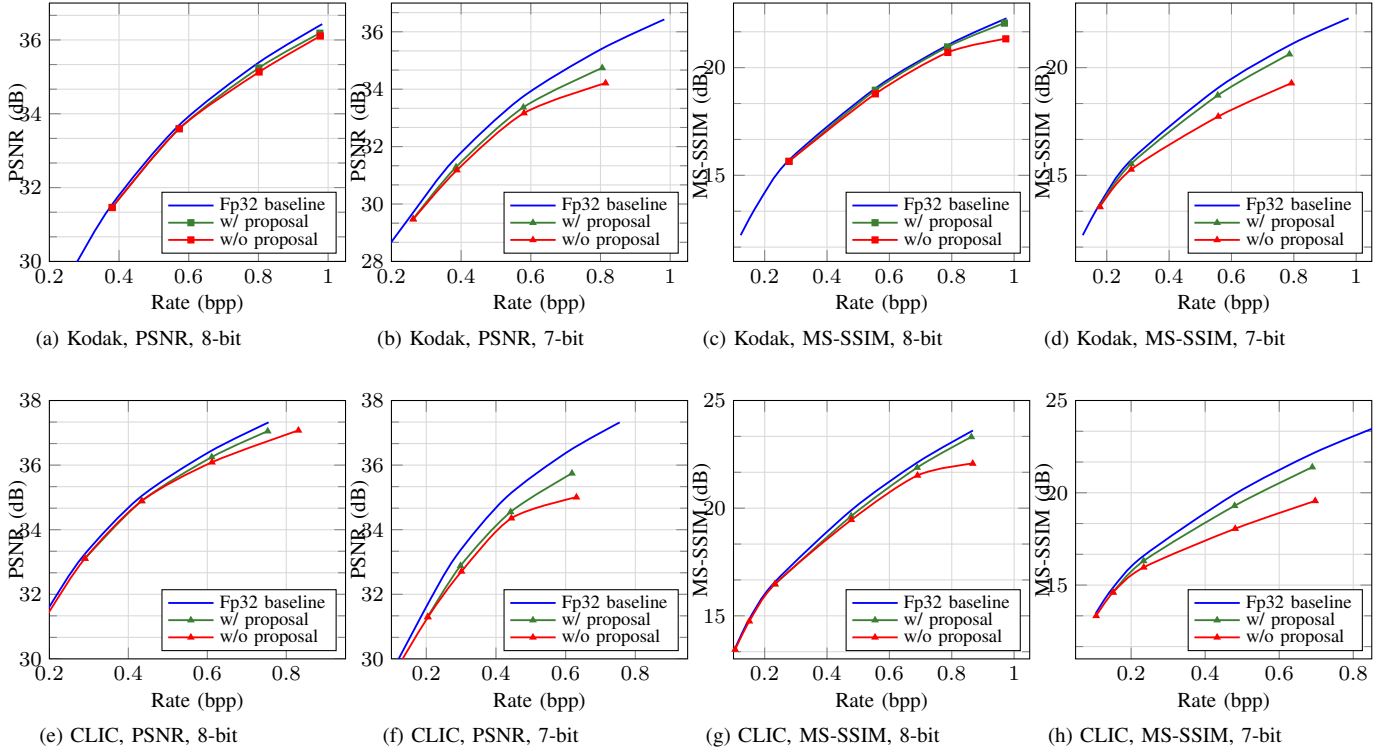


Fig. 7. Coding gain comparison of 7/8-bit activation quantization with 32-bit floating-point baseline.

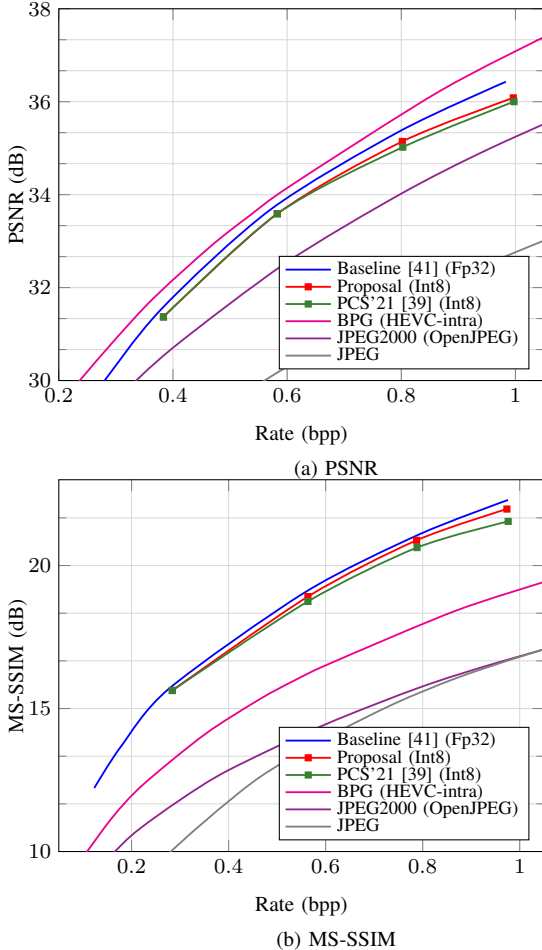


Fig. 8. Coding gain comparison with recent work [39] for a fully 8-bit QLIC framework.

TABLE II  
R-D COST COMPARISON OF OUR PROPOSAL, STATE-OF-THE-ART NETWORK QUANTIZATION METHOD [36] AND THEIR COMBINATION

Model	Quan. Bit	Method	Kodak	CLIC
0.03	7bit	Baseline	1.4071	1.1193
		w/o Proposal	1.5975	1.3059
		Proposal	1.5125	1.2119
		EWGS [36]	1.4759	1.1826
		Proposal+EWGS [36]	1.4478	1.1498
0.05	8bit	Baseline	1.7818	1.4514
		w/o Proposal	1.8405	1.5710
		Proposal	1.8279	1.4927
		EWGS [36]	1.8178	1.4796
		Proposal+EWGS [36]	1.8106	1.4752
80	7bit	Baseline	1.4064	1.1782
		w/o Proposal	1.7370	1.5827
		Proposal	1.4788	1.2706
		EWGS [36]	1.5418	1.3484
		Proposal+EWGS [36]	1.4341	1.2120
128	8bit	Baseline	1.7267	1.4203
		w/o Proposal	1.9138	1.6617
		Proposal	1.7640	1.4608
		EWGS [36]	1.8164	1.5348
		Proposal+EWGS [36]	1.7469	1.4473

## VI. CONCLUSION

This paper gives an activation quantization method for LIC. Not only the activation output of the bottleneck layer, but also non-bottleneck layer are quantized. By channel splitting, the dynamic range of channels can be reduced so that the quantization error can be reduced. However, channel splitting will lead to some incremental channels. To keep the network size as origin, channels with the smallest energy will be pruned. As a result, without any network overhead, the coding



loss can be reduced for the quantized LIC. In the future work, we will map the quantized LIC network on some specific hardwares such as FPGA. We will also quantize other LIC network structures.

## REFERENCES

- [1] G. K. Wallace, "The jpeg still picture compression standard," *IEEE Transactions on Consumer Electronics*, vol. 38, 1992.
- [2] M. Rabbani and R. Joshi, "An overview of the jpeg 2000 still image compression standard," *Signal processing: Image communication*, vol. 17, no. 1, pp. 3–48, 2002.
- [3] L. Lian and W. Shilei, "Webp: A new image compression format based on vp8 encoding," *Microcontrollers & Embedded Systems*, vol. 3, 2012.
- [4] G. J. Sullivan, J.-R. Ohm, W.-J. Han, and T. Wiegand, "Overview of the high efficiency video coding (hevc) standard," *IEEE Transactions on circuits and systems for video technology*, vol. 22, no. 12, pp. 1649–1668, 2012.
- [5] J. Ballé, D. Minnen, S. Singh, S. J. Hwang, and N. Johnston, "Variational image compression with a scale hyperprior," in *International Conference on Learning Representations*, 2018.
- [6] D. Minnen, J. Ballé, and G. D. Toderici, "Joint autoregressive and hierarchical priors for learned image compression," in *Advances in Neural Information Processing Systems*, 2018, pp. 10771–10780.
- [7] Z. Cheng, H. Sun, M. Takeuchi, and J. Katto, "Learned image compression with discretized gaussian mixture likelihoods and attention modules," *arXiv preprint arXiv:2001.01568*, 2020.
- [8] Z. Guo, Z. Zhang, R. Feng, and Z. Chen, "Causal contextual prediction for learned image compression," *IEEE Transactions on Circuits and Systems for Video Technology*, 2021.
- [9] T. Chen, H. Liu, Z. Ma, Q. Shen, X. Cao, and Y. Wang, "End-to-end learnt image compression via non-local attention optimization and improved context modeling," *IEEE Transactions on Image Processing*, vol. 30, pp. 3179–3191, 2021.
- [10] Y. Hu, W. Yang, Z. Ma, and J. Liu, "Learning end-to-end lossy image compression: A benchmark," *IEEE Transactions on Pattern Analysis and Machine Intelligence*, 2021.
- [11] Y. Wang, D. Liu, S. Ma, F. Wu, and W. Gao, "Ensemble learning-based rate-distortion optimization for end-to-end image compression," *IEEE Transactions on Circuits and Systems for Video Technology*, vol. 31, no. 3, pp. 1193–1207, 2020.
- [12] B. Bross, Y.-K. Wang, Y. Ye, S. Liu, J. Chen, G. J. Sullivan, and J.-R. Ohm, "Overview of the versatile video coding (vvc) standard and its applications," *IEEE Transactions on Circuits and Systems for Video Technology*, vol. 31, no. 10, pp. 3736–3764, 2021.
- [13] S. Ma, X. Zhang, C. Jia, Z. Zhao, S. Wang, and S. Wanga, "Image and video compression with neural networks: A review," *IEEE Transactions on Circuits and Systems for Video Technology*, 2019.
- [14] S. Han, J. Pool, J. Tran, and W. Dally, "Learning both weights and connections for efficient neural network," in *Advances in neural information processing systems*, 2015, pp. 1135–1143.
- [15] H. Li, A. Kadav, I. Durdanovic, H. Samet, and H. P. Graf, "Pruning filters for efficient convnets," *arXiv preprint arXiv:1608.08710*, 2016.
- [16] Y. He, X. Zhang, and J. Sun, "Channel pruning for accelerating very deep neural networks," in *Proceedings of the IEEE International Conference on Computer Vision*, 2017, pp. 1389–1397.
- [17] J.-H. Luo, J. Wu, and W. Lin, "Thinet: A filter level pruning method for deep neural network compression," in *Proceedings of the IEEE international conference on computer vision*, 2017, pp. 5058–5066.
- [18] X. Zhang, J. Wang, C. Zhu, Y. Lin, J. Xiong, W.-m. Hwu, and D. Chen, "Dnnbuilder: an automated tool for building high-performance dnn hardware accelerators for fpgas," in *2018 IEEE/ACM International Conference on Computer-Aided Design (ICCAD)*. IEEE, 2018, pp. 1–8.
- [19] Y.-H. Chen, T. Krishna, J. S. Emer, and V. Sze, "Eyeriss: An energy-efficient reconfigurable accelerator for deep convolutional neural networks," *IEEE journal of solid-state circuits*, vol. 52, no. 1, pp. 127–138, 2016.
- [20] X. Zhang, H. Ye, J. Wang, Y. Lin, J. Xiong, W.-m. Hwu, and D. Chen, "Dnnexplorer: a framework for modeling and exploring a novel paradigm of fpga-based dnn accelerator," in *Proceedings of the 39th International Conference on Computer-Aided Design*, 2020, pp. 1–9.
- [21] H. Ye, X. Zhang, Z. Huang, G. Chen, and D. Chen, "Hybridnn: A framework for high-performance hybrid dnn accelerator design and implementation," in *2020 57th ACM/IEEE Design Automation Conference (DAC)*. IEEE, 2020, pp. 1–6.
- [22] J. Jo, S. Cha, D. Rho, and I.-C. Park, "Dspip: A scalable inference accelerator for convolutional neural networks," *IEEE Journal of Solid-State Circuits*, vol. 53, no. 2, pp. 605–618, 2017.
- [23] S. Han, H. Mao, and W. J. Dally, "Deep compression: Compressing deep neural networks with pruning, trained quantization and Huffman coding," *arXiv preprint arXiv:1510.00149*, 2015.
- [24] A. Zhou, A. Yao, Y. Guo, L. Xu, and Y. Chen, "Incremental network quantization: Towards lossless cnns with low-precision weights," *arXiv preprint arXiv:1702.03044*, 2017.
- [25] Y. Gong, L. Liu, M. Yang, and L. Bourdev, "Compressing deep convolutional networks using vector quantization," *arXiv preprint arXiv:1412.6115*, 2014.
- [26] Y. Xu, W. Dai, Y. Qi, J. Zou, and H. Xiong, "Iterative deep neural network quantization with lipschitz constraint," *IEEE Transactions on Multimedia*, 2019.
- [27] E. Park, S. Yoo, and P. Vajda, "Value-aware quantization for training and inference of neural networks," in *Proceedings of the European Conference on Computer Vision (ECCV)*, 2018, pp. 580–595.
- [28] E. Park, J. Ahn, and S. Yoo, "Weighted-entropy-based quantization for deep neural networks," in *Proceedings of the IEEE Conference on Computer Vision and Pattern Recognition*, 2017, pp. 5456–5464.
- [29] A. Mishra, E. Nurvitadhi, J. J. Cook, and D. Marr, "Wprn: wide reduced-precision networks," *arXiv preprint arXiv:1709.01134*, 2017.
- [30] S. Jung, C. Son, S. Lee, J. Son, J.-J. Han, Y. Kwak, S. J. Hwang, and C. Choi, "Learning to quantize deep networks by optimizing quantization intervals with task loss," in *Proceedings of the IEEE Conference on Computer Vision and Pattern Recognition*, 2019, pp. 4350–4359.
- [31] Z. Cai, X. He, J. Sun, and N. Vasconcelos, "Deep learning with low precision by half-wave gaussian quantization," in *Proceedings of the IEEE Conference on Computer Vision and Pattern Recognition*, 2017, pp. 5918–5926.
- [32] S. Ioffe and C. Szegedy, "Batch normalization: Accelerating deep network training by reducing internal covariate shift," *arXiv preprint arXiv:1502.03167*, 2015.
- [33] S. Lloyd, "Least squares quantization in pcm," *IEEE transactions on information theory*, vol. 28, no. 2, pp. 129–137, 1982.
- [34] J. Choi, Z. Wang, S. Venkataramani, P. I.-J. Chuang, V. Srinivasan, and K. Gopalakrishnan, "Pact: Parameterized clipping activation for quantized neural networks," *arXiv preprint arXiv:1805.06085*, 2018.
- [35] Z. Zhou, W. Zhou, X. Lv, X. Huang, X. Wang, and H. Li, "Progressive learning of low-precision networks," *IEEE Transactions on Multimedia*, 2020.
- [36] J. Lee, D. Kim, and B. Ham, "Network quantization with element-wise gradient scaling," in *Proceedings of the IEEE/CVF Conference on Computer Vision and Pattern Recognition*, 2021, pp. 6448–6457.
- [37] J. Ballé, N. Johnston, and D. Minnen, "Integer networks for data compression with latent-variable models," in *International Conference on Learning Representations*, 2019.
- [38] H. Sun, Z. Cheng, M. Takeuchi, and J. Katto, "End-to-end learned image compression with fixed point weight quantization," in *2020 IEEE International Conference on Image Processing (ICIP)*. IEEE, 2020, pp. 3359–3363.
- [39] H. Sun, L. Yu, and J. Katto, "Learned image compression with fixed-point arithmetic," in *2021 Picture Coding Symposium (PCS)*. IEEE, 2021, pp. 1–5.
- [40] W. Hong, T. Chen, M. Lu, S. Pu, and Z. Ma, "Efficient neural image decoding via fixed-point inference," *IEEE Transactions on Circuits and Systems for Video Technology*, 2020.
- [41] Z. Cheng, H. Sun, M. Takeuchi, and J. Katto, "Deep residual learning for image compression," *IEEE Conference on Computer Vision and Pattern Recognition Workshop and Challenge on Learned Image Compression*, pp. 1–5, 2019.
- [42] J. Ballé, V. Laparra, and E. P. Simoncelli, "End-to-end optimized image compression," *arXiv preprint arXiv:1611.01704*, 2016.
- [43] J. Katto and Y. Yasuda, "Performance evaluation of subband coding and optimization of its filter coefficients," *Journal of visual communication and image representation*, vol. 2, no. 4, pp. 303–313, 1991.
- [44] N. S. Jayant and P. Noll, "Digital coding of waveforms: principles and applications to speech and video," *Englewood Cliffs, NJ*, pp. 115–251, 1984.
- [45] S. Savchev and T. Andreescu, *Mathematical miniatures*. MAA, 2003, vol. 43.
- [46] R. Franzen, "Kodak lossless true color image suite," *source: http://r0k.us/graphics/kodak*, vol. 4, 1999.
- [47] G. Bjontegaard, "Calculation of average psnr differences between rd-curves," *VCEG-M33*, 2001.